Ocean Engineering 144 (2017) 203–210

Contents lists available at ScienceDirect

Ocean Engineering

journal homepage: www.elsevier.com/locate/oceaneng

Insight into the lateral response of offshore shallow foundations

A. Barari[a,b,*], L.B. Ibsen[a]

[a] Department of Civil Engineering, Aalborg University, Thomas Manns Vej 23, 9220 Aalborg Ø, Denmark
[b] Department of Civil and Environmental Engineering, Virginia Tech, Blacksburg, VA, USA

ARTICLE INFO

Keywords:
Suction caissons
Densification
Cyclic loading
Impedance
Stiffness

ABSTRACT

Suction caissons are often subjected to cyclic lateral loads caused by the action of wind or waves. As a result of these cyclic loads, excessive lateral deformations may be induced during a caisson's service life. Although soil-foundation response analysis requires information about stiffness and damping at the site, the methods for obtaining this information are still in question. The present study reports non-dimensional frameworks for determining the impedance functions for soil-foundation system at the load reference point along with the results of performance measure parameters that track the response of suction caissons harmonically oscillating on homogeneous soil. The equations are expressed in terms of logarithmic and polynomial models based on a statistical analysis of existing cyclic test results for small-scale Aalborg University Instrumented Suction Caissons, 300 mm in diameter and 300 mm in skirt length.

The variables used in the equations for normalized secant stiffness are load characteristics (ξ_b and ξ_c) and number of load cycles. The present study also identifies critical new findings regarding the local densification and the plastic shake-down at the caisson-soil interface, which are all important factors to consider in a performance based-framework for designing offshore structures.

1. Introduction

By 2004, more than 485 suction anchors had been installed at over 50 different sites (Andersen et al., 2005). Most of these anchors are in clay, but some are in sand or layered soil. Examples of skirted foundations in sand are the offshore platforms at the Draupner E and Sleipner T sites in the North Sea (Tjelta, 1995).

Recently there has arisen a salient trend in the construction of modern wind turbines with a slender design and more than 100 m in tower height; the natural frequencies of these rather novel structures are close to 0.2 Hz. Fig. 1 compares the average water depths for wind farms that are currently in the design phase. The transition to deeper water increases the span between the turbine superstructure and the seabed. Coupled with greater environmental loading from the higher-magnitude wind and waves, the move to deeper water increases the moments applied to the foundations. While monopiles are attractive solutions for developers and designers alike, the increased water depth requires larger diameters with stiffer cross-sections. The monopiles used to date consists of a stiff pile of diameter of 4–6 m and embedment depths ranging from 20 to 30 m. In 2008, Ibsen reported the performance of a bucket foundation installed in Frederikshavn, Denmark as an attractive alternative foundation which can be used to increase the moment capacity (Ibsen, 2008). The bucket foundation, also referred to as "suction caisson", is a large cylindrical monopod foundation, typically made of steel (Fig. 2) which has the potential to be a cost effective option in certain soil conditions. A bucket foundation typically requires less steel compared to a monopile, but fabrication costs are slightly higher due to the complicated lid structure (Table 1). However, the total cost, steel and fabrication, of a bucket foundation is likely to be less than of a monopile. Typical loading conditions for an offshore bucket foundation are illustrated schematically in Table 2. The loads are shown to be acting at the interface level between the foundation and the turbine shaft. An axial load of approximately 264 t act at this point.

This foundation is an upside-down bucket made of steel with diameter D, skirt length d and skirt wall thickness t. A standard real-scale foundation for a 5 MW wind turbine has $D = 12–18$ m, $t \approx 30$ mm and embedment ratio ranging between 0.5 and 1.

Motion of a bucket foundation will induce forces transmitted through the foundation-soil contact elements into the underlying deformable ground, which produce cyclic strains in terms of displacements and rotation of the foundation. Under a moderate to high amplitude of cyclic loading, most soils change stiffness and damping. In order to study the long-term performance and the uncertainties related to the dynamic response of these structures, the soil stiffness due to these cyclic strains must be taken into consideration. The current codes

* Corresponding author at: Department of Civil Engineering, Aalborg University, Thomas Manns Vej 23, 9220 Aalborg Ø, Denmark.
E-mail address: abarari@vt.edu (A. Barari).

http://dx.doi.org/10.1016/j.oceaneng.2017.08.012
Received 26 October 2015; Received in revised form 28 June 2017; Accepted 8 August 2017

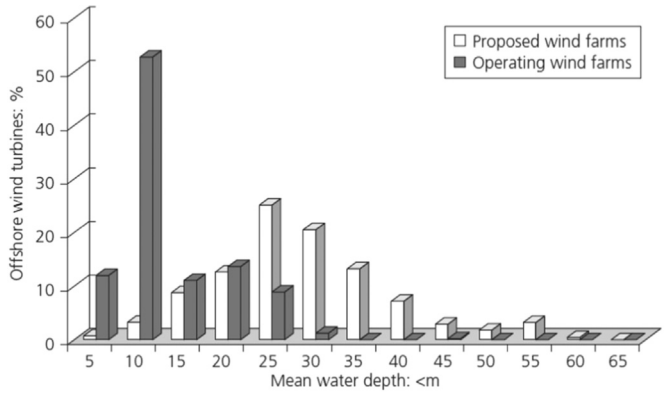

Fig. 1. Water depth for future and in-service wind farms (Doherty and Gavin, 2011).

Fig. 2. Prototype Bucket foundation prior to installation.

Table 1
Cost make up for 8 MW bucket foundation and equivalent monopile (Nielsen, 2014).

Water depth (m)	Steel required for bucket foundation (ton)	Steel required for equivalent monopile (ton)
25	610	820
35	760	–
45	980	–
55	1200	–

Table 2
Details of a typical suction caisson-supported Vestas 3.0 MW wind turbine (Ibsen, 2014).

Component		
Rotor	Diameter	90 m
	Nominal rev.	16.1 rpm
Tower	Hub Height	80 m
Weight	Tower	156 t
	Nacelle	68 t
	Rotor	40 t
	Total	264 t
Foundation	Diameter	12 m
	Height	6 m
	Weight	135 t

of practice (API, ISO and DNV) for the design of offshore foundations provide limited guidance for predicting changes in the foundation stiffness and the resulting changes in damping, which are important design drivers for serviceability limit state (SLS) and fatigue limit state (FLS) requirements.

Experimental studies provided the data necessary to establish combined loading interaction (Bransby and Randolph, 1999; Gourvenec, 2008; Nova and Montrasio, 1991; Houlsby and Cassidy, 2002; Cassidy et al., 2002, 2004; Bienen et al., 2006; Villalobos, 2006; Ibsen et al., 2014a, 2014b, 2015; Barari and Ibsen, 2012, 2014; Larsen et al., 2013). The programmes of Houlsby and Cassidy (2002), Cassidy et al., (2002, 2004) and Ibsen et al. (2014a), (2014b), (2015) resulted in strain hardening models that describe the behavior of circular footings in terms of the combined forces acting on them (V, M, H) and their resulting displacements (w, θ, u). However, in these experiments only monotonic response was studied. To ensure confidence for performance of in-service shallow foundations, further studies on cyclic loading response are required. Modeling significant change in soil-foundation stiffness, derived for the idealized case of a suction caisson fully bonded at the soil surface, is therefore of keen interest in the present study. This paper provides insight into predicting the response of cyclic lateral loading of suction caissons, and presents a complete set of non-dimensional formulas for impedance functions covering the translational mode of cyclic nature of soil-foundation behavior at a given frequency. The procedure is based on a review of previously published general procedures and a statistical analysis of laboratory test data.

To examine the effects of loading shape, load characteristics were defined as in Eq. (1):

$$\begin{cases} \xi_b = \frac{M_{\max}}{M_R} \\ \xi_c = \frac{M_{\min}}{M_{\max}} \end{cases} \quad (1)$$

where $M_{\max}$ and $M_{\min}$ are the maximum and minimum moment in the load cycle and M_R = static capacity at a given load path. As depicted in Fig. 3, ξ_c distinguishes between one-way and two-way loading. In other words, ξ_c may change in a domain ranging from 0 for one-way loading to −1 for full-two way loading.

1.1. Dynamic considerations of soil-foundation interaction in offshore wind turbines

Wind turbines are designed to have natural frequencies in the range between frequency bands of the rotor rotation and the blade passing, usually denoted by 1p and 3p (for a three-bladed turbine). This may be attributed to the various complex interactions between the structure, foundation, soil and the fluid. In particular, the main source of excitation is the rotor blades passing tower and is very close to the first natural frequency. This hypothesis has also drawn considerable attention in codes of practice. Accurately modeling the dynamic stiffness of the structure is required to predict the dynamic response and the fatigue lifespan of a wind turbine.

For pile foundations, limited previous research using small scale 1 g-tests (Lombardi, 2010; Bhattacharya et al., 2011, 2012) has examined whether the natural frequency of a wind turbine may change with cycles of loading; this research revealed significant change in soil stiffness which changed the first natural frequency of the wind turbine and caused it to approach excitation frequencies. Alteration of the foundation stiffness may be attributed to either strain-hardening or softening, owing to vibration of the soil-foundation systems (LeBlanc et al., 2010). For strain hardening sites where the stiffness increases, the natural frequency of the system will also increase. On the other

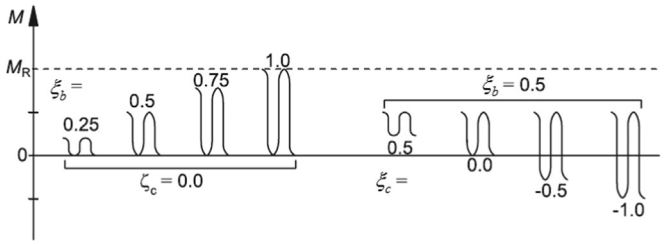

Fig. 3. Cyclic load characteristics.

hand, for strain-softening sites, where the stiffness of the soil may decrease with each cycle, natural frequency will also decrease accordingly.

A key step in the dynamic analysis of soil-foundation systems under cyclic loads is to use experimental, analytical or numerical methods to estimate the dynamic impedance functions that are associated with a rigid foundation. For a rigid suction caisson, the steady-state response to harmonic external forces can be determined once the matrix of dynamic impedance functions has been determined for the frequency of interest.

Over the previous years, a series of alternative design schemes have been developed for foundation impedances (Luco, 1982; Gazetas, 1983; Lysmer and Richart, 1966; Kagawa and Kraft, 1980; Mita and Luco, 1989).

The selection of an appropriate method for a given application depends on key characteristics of the foundation-soil interface and of the excitation (Banerjee and Butterfield, 1987), which are: the shape of the foundation-soil interface, the embedment ratio, the nature of the soil profile, and the mode of vibration.

1.2. Definition of impedances

For a specific harmonic excitation, the dynamic impedance is defined as the ratio between a force (or moment) R and the resulting steady-state displacement (or rotation) U at the bucket load reference point.

There are generally eight different impedances covering six possible modes of vibration of the rigid foundation: two horizontal (s_x and s_y); one vertical (s_z); one torsional (s_t); and two rocking (s_{rx} and s_{ry}). Horizontal forces acting on principal axes induce cross-coupling horizontal-rocking impedances s_{xry} and s_{yrx}. This effect is more pronounced for greater embedment depths (Banerjee and Butterfield, 1987).

It is convenient to introduce complex notation and to express each type of impedance in the form of Eq. (2).

$$S = \overline{K} + i\omega C \tag{2}$$

The real component $\overline{K}$ is termed the dynamic stiffness and inertia of the supporting soil; its dependence on frequency is attributed solely to the influence of that frequency on inertia. The imaginary component, ωC, is the product of frequency ω and the dashpot coefficient C. Eq. (2) simplifies the foundation-soil system as a spring-dashpot supported foundation with characteristic moduli equal to $\overline{K}$ and C, respectively.

For frequency-dependent excitation, the dynamic stiffness matrix is defined by Eq. (3) (Andersen et al., 2008):

$$\begin{bmatrix} V/G_sR^2 \\ H_1/G_sR^2 \\ H_2/G_sR^2 \\ T/G_sR^2 \\ M_1/G_sR^3 \\ M_2/G_sR^3 \end{bmatrix} = \begin{bmatrix} K_{VV} & 0 & 0 & 0 & 0 & 0 \\ 0 & K_{HH} & 0 & 0 & 0 & -K_{HM} \\ 0 & 0 & K_{HH} & 0 & K_{HM} & 0 \\ 0 & 0 & 0 & K_{TT} & 0 & 0 \\ 0 & 0 & K_{MH} & 0 & K_{MM} & 0 \\ 0 & -K_{MH} & 0 & 0 & 0 & K_{MM} \end{bmatrix} \begin{bmatrix} W/R \\ U_1/R \\ U_2/R \\ \theta_T \\ \theta_{M1} \\ \theta_{M2} \end{bmatrix} \tag{3}$$

where G_s is the shear modulus of the soil. The sign convention for displacements and loads presented in this paper obey a right-handed axis and clockwise positive convention as proposed by Butterfield et al. (1997) for a shallow foundation under three-degrees-of-freedom loading (Fig. 4).

Thereby, stiffness matrix for offshore shallow foundations subjected to planar loading may be simplified by the following components:

$$\begin{bmatrix} V/GR^2 \\ H/GR^2 \\ M/GR^2 \end{bmatrix} = \begin{bmatrix} K^0{}_{VV} & 0 & 0 \\ 0 & K^0_{HH} & K^0_{HM} \\ 0 & K^0_{HM} & K^0_{MM} \end{bmatrix} \begin{bmatrix} W/R \\ U/R \\ \theta_M \end{bmatrix} \tag{4}$$

where R is the radius of the foundation, and $K^0{}_{ij}$ are the non-dimensional static stiffness components.

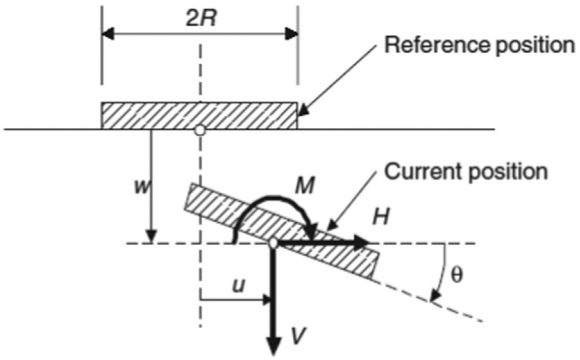

Fig. 4. Sign conventions for 3 degree-of-freedom loading (Butterfield et al., 1997).

2. Experimental procedure

The experimental program spanned from 2011 to 2013 at Aalborg University and included tests performed using instrumented model caisson.

The arrangements used for tests are shown in Fig. 5. All experiments were carried out at 1 g and involved the application of cyclic sinusoidal lateral loads to a tower at a normalsied height of M/HD=2 above the base of footing. Two load cells were mounted on the tower to record the cyclic loads. The model caisson was constructed by using a 0.3 m external diameter open-ended hollow cylinder with wall thickness t=1.5 mm and stainless steel and consisted of a 0.3 m skirt length instrumented section that housed three linear variable differential transformers (LVDTs) and pore pressure sensors.

This footing diameter is equivalent to 15 m at prototype scale (i.e., scale ratio = 1/50) supporting a 5 MW wind turbine installed in dense silica sand. Details of the foundation tests and loading parameters are given in Table 3.

The cyclic stress ratio (CSR) of the soil elements in the vicinity of the foundation corresponds to a resultant cyclic load ratio (CLR) of the whole caisson-soil system which is the ratio of the cyclic load amplitude to the static bearing capacity of caisson. Two non-dimensional parameters, ξ_b which is practically equal to CLR and ξ_c for different tests are also listed in Table 3.

The sand used was uniformly graded fine silica sand with a mean effective particle size (D_{50}) of 0.14 mm and void ratio limits of 0.549 and 0.858. This sand was air pluviated into a 1600 × 1600 × 1150 mm^3 sand box and then saturated slowly before being vibrated to achieve a dense consistency. The water level was maintained coincident with the ground level throughout the experimental program.

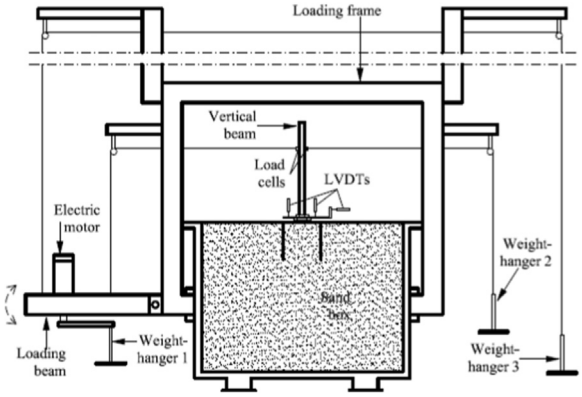

Fig. 5. Experimental setup for 1 g- experiments on suction caissons.

Table 3
Cyclic Test Program.

Test No.	h (mm)	d/D	M_{min} (N m)	M_{max} (N m)	ξ_b	ξ_c	No. of cycles	Relative density, R_D
MB-C17	596	1	2.66	98.26	0.54	0.02	49,978	79.62
MB-C18	596	1	−2.33	55.71	0.3	−0.04	50,004	90.71
MB-C20	596	1	−39.07	65.7	0.36	−0.6	50,049	82.67
MB-C22	596	1	13.58	70.26	0.38	0.19	50,255	82.33
MB-C23	596	1	−29.73	69.84	0.38	−0.43	50,209	86.71
MB-C24	596	1	−64.77	67.28	0.38	−0.96	50,642	83.09
MB-C31	596	1	2.26	62.16	0.34	0.04	100,933	91.20
MB-C32	596	1	−11.48	77.21	0.42	−0.15	49,959	92.65
MB-C33	596	1	−22.16	70.13	0.38	−0.32	50,471	92.09
MB-C35	596	1	−48.04	88.8	0.48	−0.54	9976	88.87
MB-C36	596	1	−60.18	106.84	0.58	−0.56	10,153	98.79
MB-C37	596	1	−72.54	126.03	0.69	−0.58	10,083	99.41
MB-C40	596	1	−99.31	211.84	1.156	−0.469	108	96.17
MB-C47	596	1	−55.23	69.35	0.38	−0.79	50,001	96.9

3. Performance based design: typical results

3.1. Variation of bucket stiffness: non-dimensional framework

Since this paper aspires to characterize the global soil-foundation response in performance-based design terms, this section provides several insights regarding dynamic properties as well as useful inputs for applications of performance-based evaluation.

The cohesionless soil exhibits dilatancy at low stress levels (e.g., laboratory tests at 1 g) which in turn may be associated with higher friction angle than soil with the same relative density in the field (Guo and Qin, 2010; LeBlanc et al., 2010).

With this limitation to this study in mind, Fig. 6 depicts the tangent and secant stiffness at each unloading-reloading reversal point. Fig. 7 outlines the non-dimensional form of tangent and secant stiffness obtained at each unloading–reloading reversal point and the sequential reversal points, respectively divided by corresponding stiffness at the first cycle. They are defined here as the ratio of the lateral load to the reference point lateral displacement at the soil-foundation interaction.

Although the results are somewhat inconclusive due to the existence of large scatter in the tangent stiffness data, unaffected by the load path, the secant stiffness is much smaller than those in subsequent cycles. This observation opposes the current methodology of degrading static p-y curves (Barari et al., 2015) to account for cyclic loading. After a tremendous increase in the first cycle, the $\sim K_{s,n}$ (i.e., lateral secant cyclic stiffness at cycle N) increases slightly with the increasing number of load cycles but at reduced rate, as shown in Fig. 7. The increase in the measured stiffness may be attributed to soil densification during cyclic loading. It is worthy of note that the roughly nonlinear behavior during the tests causes a gradual increase in $K_{s,n}$. Given that the amplitude of cyclic loads was large enough to trigger soil hardening, the largest value of $K_{s,n}$ in all tests is about 1694 N/mm after cyclic loading.

The results for a series of load groups, plotted in Fig. 7, show a very good fit to a logarithmic expression. The results approximately include 10^4 load cycles. Plotting non-dimensional secant stiffness as a function of $\ln(N)$ suggests that stiffness evolves logarithmically with cycle number as:

$$\tilde{k} = \frac{K_{s,n}}{K_{s,1}} = \tilde{k}_0 + A_k \ln(N) \tag{5}$$

where $\tilde{k}_0$ and A_k are correlation coefficients. This study adopted the values of $\tilde{k}_0$ and A_k determined by multiple regression, which provide the best fit between Eq. (5) and the data in Fig. 7. Least-squares regression of all the test results yields A_k equal to 0.14, which implies that A_k is independent of the load characteristics over the observed range. On the other hand, $\tilde{k}_0$ was determined as a function of the load characteristics.

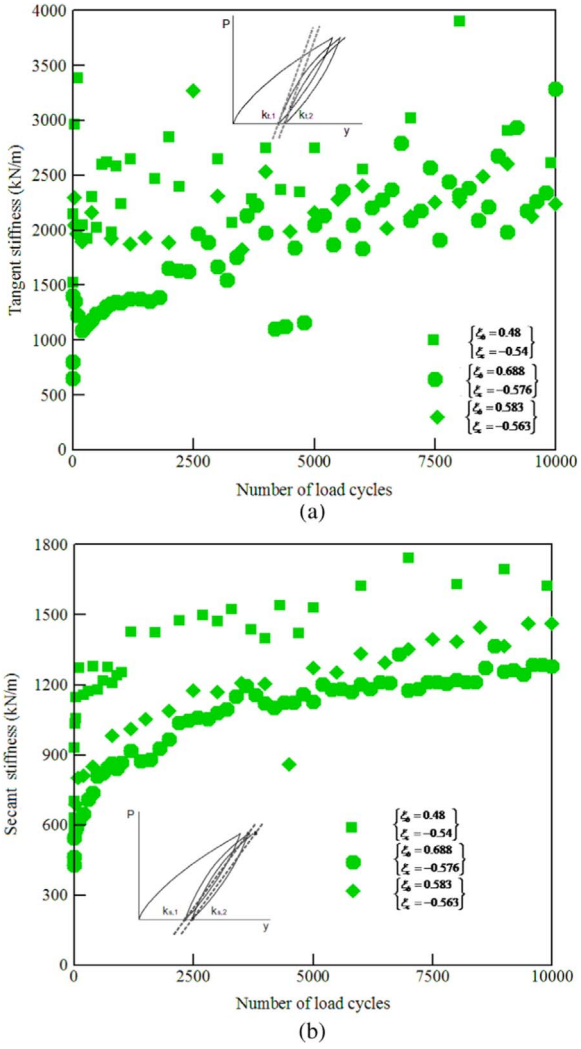

Fig. 6. Bucket lateral stiffness: (a) tangent stiffness (b) secant stiffness.

The empirically determined values of $\tilde{k}_0$ can be expressed by Eq. (6):

$$\tilde{k}_0 = k_b(\xi_b)k_c(\xi_c) \tag{6}$$

in which k_b and k_c are dimensionless functions, depending on the load characteristics. The function k_c is defined such that $k_c(\xi_c = 0) = 1$. The empirically determined values of k_b and k_c are illustrated as functions of ξ_b and ξ_c, respectively in Figs. 8 and 9.

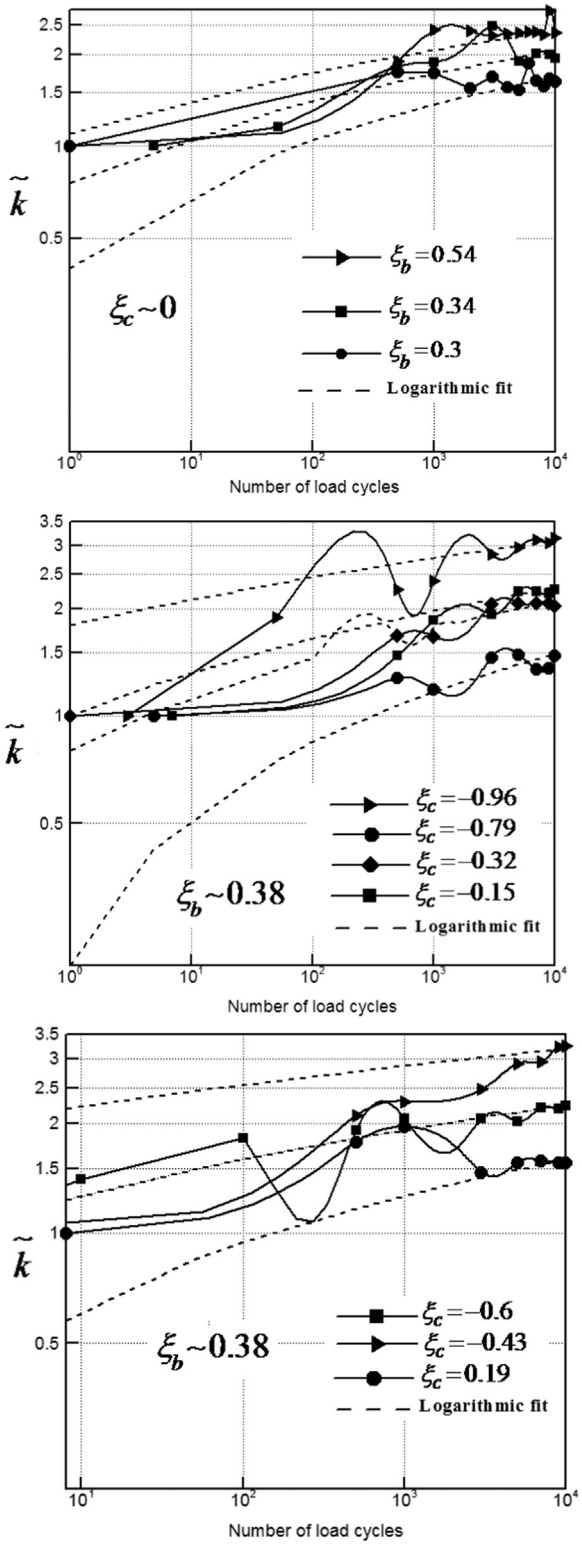

Fig. 7. Normalized bucket secant lateral stiffness.

The expression for k_b over the range ξ_b can be described by a quadratic function as in Eq. (7):

$$k_b(\xi_b) = 0.79\xi_b^2 + 2.069\xi_b - 0.009 \quad \xi_b \leq 0.6 \tag{7}$$

Fig. 8 indicates that k_b depends roughly linearly on the magnitude of the loading, (ξ_b). While one-way load cycling involves applying cyclic loads for only one sign, it is likely to generate full mobilisation of the

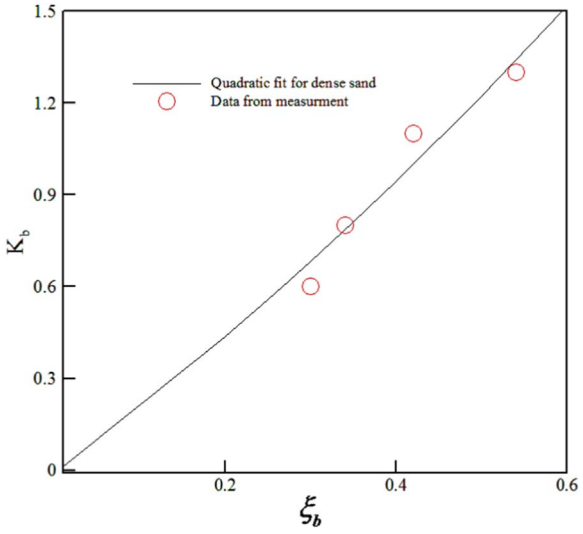

Fig. 8. Fitted empirical constant k_b against the ξ_b.

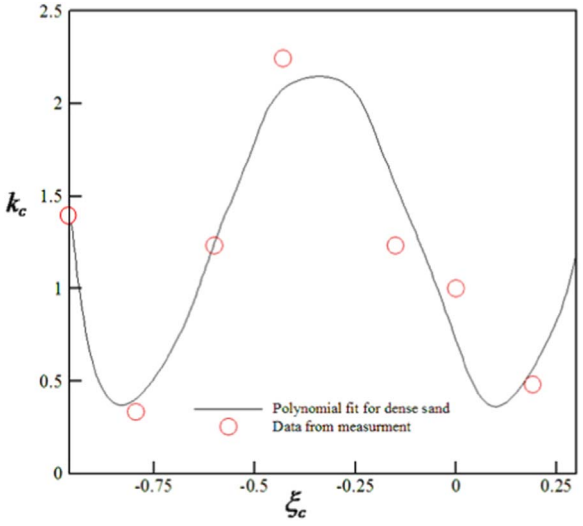

Fig. 9. Fitted empirical constant k_c against the ξ_c.

lateral soil resistance, especially at higher load levels. Fig. 9 implies that the largest evolved stiffness occurs for ξ_c = −0.5 which, interestingly, compares to the value ξ_c = −0.7 used by Zhu et al. (2013) for accumulated rotation of suction caissons. A less evolved stiffness must be expected for one-way loading, since much higher load levels are expected for two-way loads. It is worth noting that at small strain deformations, the potential for the change in foundation stiffness trends depends on the complexities of loading patterns. Low-level cycling at small strain deformations may have negative effects on foundation capacity, leading to less symmetry and a local stiffness loss. Foglia and Ibsen (2014) concluded that lateral post-cyclic bearing capacity of suction caissons can benefit on average 10.5% from stable cycling. Further investigations are needed to verify this hypothesis.

Plotted in the Fig. 9 is the polynomial function which best fits the data for k_c due to cyclic loading (Eq. (8)):

$$k_c(\xi_c) = 39\xi_c^4 + 53.6\xi_c^3 + 10.89\xi_c^2 - 5.22\xi_c + 0.72 \quad -1 \leq \xi_c \leq 0.25 \tag{8}$$

3.2. Relative displacements

The stability of the soil-foundation system for lateral response of buckets in sand is investigated by analyzing the accumulation rate of

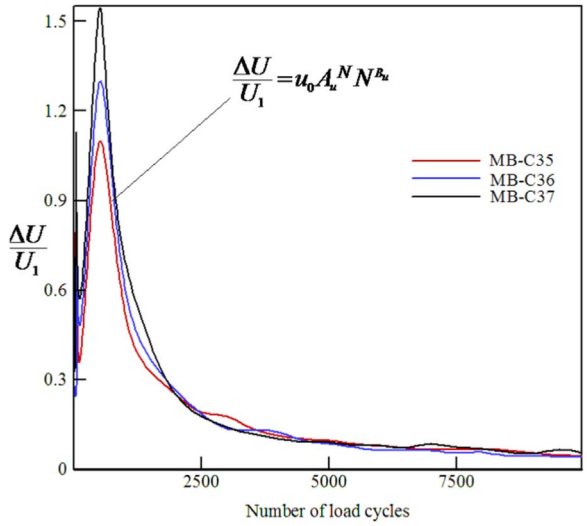

Fig. 10. Relative bucket head displacement between two consecutive re-loading unloading reversal points normalized with the one between the virgin loading and the first re-loading unloading reversal point ($\tilde{u}_0$, A_u and B_u are correlation coefficients).

plastic displacement. Fig. 10 presents the relative bucket head displacement between two subsequent re-loading un-loading reversal points, normalized with the one between virgin loading-unloading and the first reloading-unloading reversal points. Typical results from tests MB-C35, MB-C36 and MB-C37 show that the accumulation rate of plastic displacement decreased as the number of load cycles increased, indicative of the stable response of the system reaching a plastic shakedown equilibrium.

3.3. Stability analysis

This section focuses on cyclic failure characteristics and identifying buckets that have been subjected to stable cycles, using the stability terminology described in Jardine and Standing (2012):

- Stable behavior: Foundation head displacements accumulate slowly over hundreds of cycles under either tension or compression (one-way) or tension followed by compression (two-way).
- Unstable behavior (US): Displacements develop rapidly leading to failure at $N\langle 100$ due to capacity losses.

Doherty and Gavin (2012) defined the stability of cyclic loaded foundations by Eq. (9), where U is the foundation displacement.

$$\begin{aligned} &stable: \quad \frac{d^2U}{dN^2}\langle 0 \\ &unstable: \quad \frac{d^2U}{dN^2}\rangle 0 \end{aligned} \tag{9}$$

Figs. 11 and 12 illustrate results from the stable cyclic tests MB-C35 and MB-C36, along with MB-C37. A noteworthy finding that emerged from the analysis of lateral force-displacement hysteresis curves of MB-C37 test is that the slender and immobile load-displacement loop was set up after approximately the first 10 cycles. The permanent displacements grew steadily by just 5.3 mm over the first 1000 cycles of two-way compression-tension cycling, but then stabilized as N increased to 10,000, with stick-slip fluctuations between ~ 210 and ~ 240 N.

Fig. 13 illustrates the load-displacement data of an exemplar two-way very high-level cyclic test, MB-C40, over the 108 cycles. The value of ξ_b = 1.15 was chosen from the measurements to obtain a static monotonous load of about 335 N. The permanent displacements grew by just 7.38 mm over the first batch of loading equal to 40 cycles, and then almost stabilized during the subsequent 40 cycles and 28 cycles.

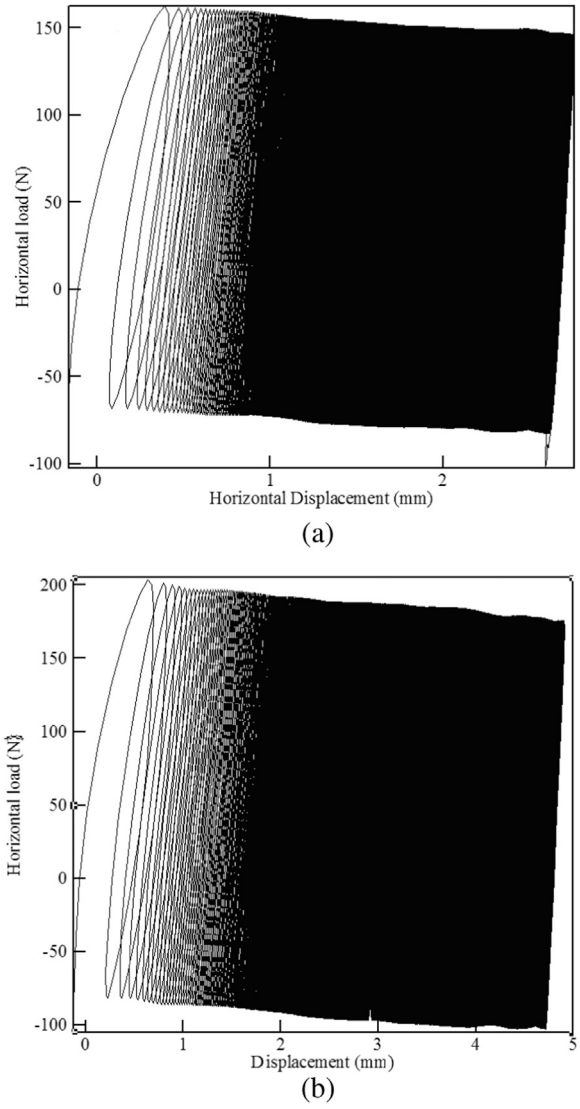

Fig. 11. The load-displacement response at load reference point during cyclic lateral load tests (a) MB-C35 (b) MB-C36.

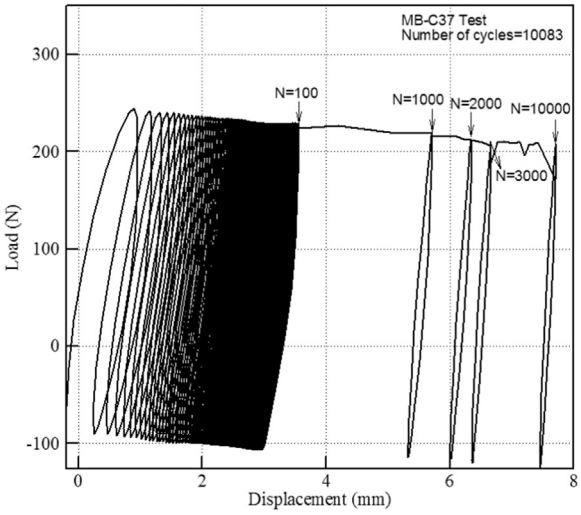

Fig. 12. Load-displacement curves over 10,000 cycles for a typical stable compression-tension cyclic test (MB-C37).

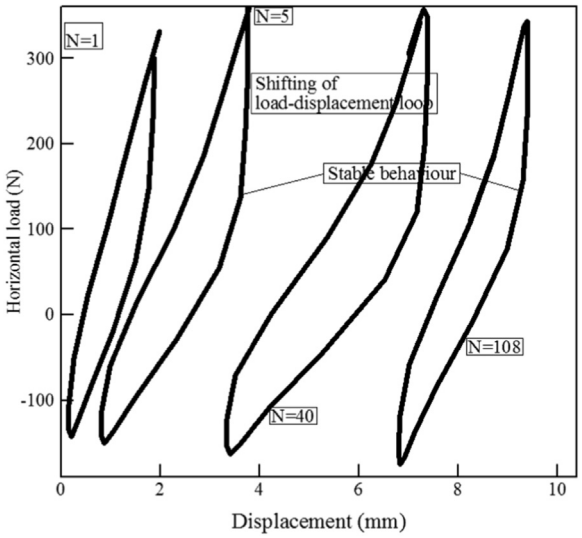

Fig. 13. Stability performance of bucket in MB-C40 test.

This stabilization observed within the test is attributed to soil-foundation system densification due to gradual enlargement of the resisting soil to surrounding area with cyclic loading. Stable cyclic loading led to a net displacement of 6.8 mm representing a total movement of < 2.3% of the bucket diameter.

In incremental form, the displacement term in the Nth cycle, U_N is decomposed into an elastic and plastic part (Chen et al., 2015):

$$U_N = (U_{Ne} + U_{Np}) = U_{(N)\max} - U_{(N-1)\min} \tag{10}$$

where $U_{(N)\max}$ is peak displacement of the caisson in the Nth cycle and $U_{(N-1)\min}$ is the residual displacement of the caisson after (N-1) cycles.

Note that the relationship for the elastic displacement term is represented as follows:

$$U_{Ne} = U_{(N)\max} - U_{(N)\min} \tag{11}$$

Fig. 14 depicts the portion of the elastic displacement to the total displacement for each cycle according to model MB-C35 response. During the moderate cycling, MB-C35, 77–91% of the elastic displacement occurred within 10 cycles in this experiment, after which caisson essentially undergoes elastic deformation. Most of plastic displacements were shown to occur over initial cycling with a smaller contribution resulting from densification of the cohesionless soil surrounding the caisson.

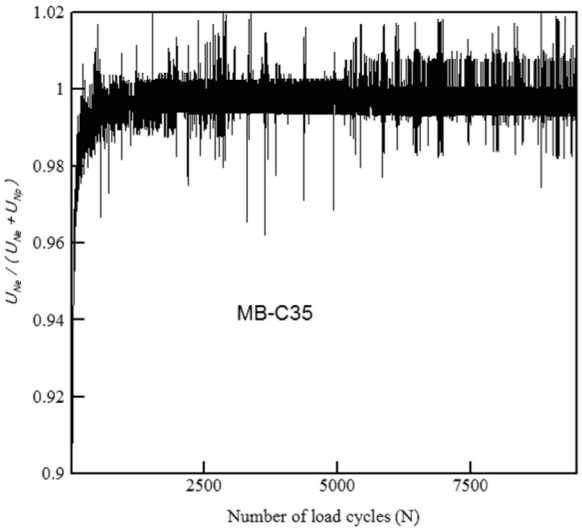

Fig. 14. Contribution of elastic displacement to the total displacement over moderate cyclic test, MB-C35.

The effects of these displacements mechanisms and their relative contribution to the total lateral displacement of soil-foundation system are expected to be a function of the soil and structural properties and the load characteristics.

3.4. Damping relationships

The damping calculated in a load test results from both radiation damping and hysteretic damping. As explained by Gazetas (1975), radiation damping occurs as energy is absorbed into the soil; waves radiate out from the point of loading and propagate through the soil medium. On the other hand, hysteretic damping accounts for the energy dissipated in the soil due to viscosity and plastic deformations as the soil is loaded and unloaded.

The total energy loss from radiation and hysteresis damping can be calculated by (Rollins et al., 2009):

$$D = \frac{W_D}{2\pi K u^2} \tag{12}$$

where W_D is the energy dissipated in one cycle of loading corresponding to the area inside the hysteresis loop; K is the stiffness in units of force/length and is calculated by the change in force over the change in displacement ($\frac{\Delta F}{\Delta U}$); and u is the single amplitude displacement (Rollins et al., 2009).

At higher strains, nonlinearity in the stress-strain relationship, along with local densification, decreases the imaginary parts of the dynamic stiffness while increasing strain amplitude in the soil medium.

Computed damping values for the three simulations are displayed in Fig. 15, where it is evident that (1) the measured lateral deformations at the first cycles corresponding to higher load levels are larger than intermediate levels; and (2) the extent of lateral deformation in this uniform profile is somehow inversely proportional to the D. As a result, higher lateral deformation (0.25 mm in MB-C37) results in smaller D. At the load reference point, the profile with the lowest lateral translation (MB-C35, 0.08 mm) had a value of D about 1.77 times that of the profile with the highest ξ_b values.

However, the relation between D and ξ_b is less apparent for subsequent load cycles. As N increases, the D values appear to decrease towards an asymptotic value, even during large-amplitude oscillation. Additional studies are needed to examine this variation with respect to the foundation diameter and skirt length.

As shown in Fig. 15, a possible linear relationship is observed between N and the small strain damping; this relationship can be expressed as follows:

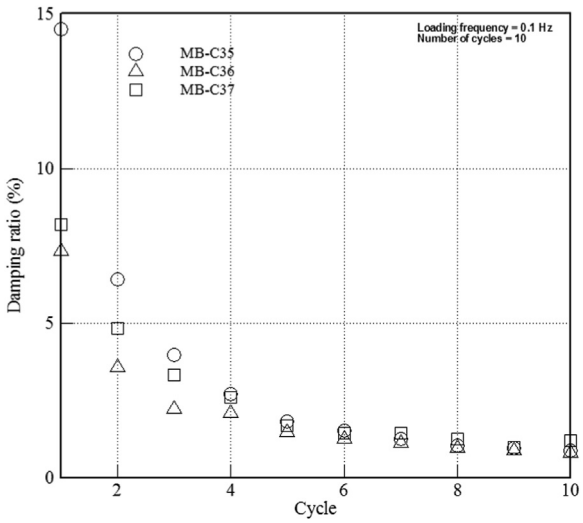

Fig. 15. Silica sand damping ratio at small strains for different load groups.

$$D = aN + b \quad (13)$$

where a and b are fitting parameters equal to about 0.69 and −0.75, respectively.

4. Conclusions

Summarized in this paper is a procedure for estimating the variation of $\tilde{k}$ and D with horizontal displacement and time for sandy soils. The procedure is based on a review of previously published general procedures and a statistical analysis of existing laboratory test data from multiple cyclic loading experiments performed on suction caissons founded on dense silica sand.

Main conclusions follow:

1. This study bridges the gap between suction caisson-soil interaction at nearly small displacements and at large deformations (plastic response) upon cyclic loading that are usually neglected in offshore foundations analyses.
2. Accordingly, appropriately defined performance measure parameters are introduced to evaluate the caisson response to distinguish between contribution of soil densification and plastic shakedown mechanism.
3. Interaction diagrams exhibits how the cyclic loading parameters, N, ξ_b and ξ_c affect cyclic response. The plots and simplified design procedures captured key aspects of the tests performed.
4. High-level cycling under one-way and two-way conditions invoked roughly different responses. The latter gave scope for higher normalized cyclic loading levels that promoted more cyclic stiffness increase rates, while the former led to less symmetric and stiffness increase.
5. Low-level cycling may have less beneficial effects on caisson capacity, and can self-heal at large strains after modest losses of stiffness which in turn high level cyclic loading can impact very significantly on lateral capacity of caissons after applying huge number of cyclic loading in model tests.
6. It can also be observed that even though there were much reduction in imaginary part at first batch of loading with the introduction of the hardening of the soil medium, the reduction in damping is so insignificant at larger strains for given low frequency range.
7. In line with the above findings, it is suggested that $\tilde{k}$ and D should be measured at frequencies and number of loading cycles similar to those of the anticipated cyclic loading from the wave and wind action to account for the effects of these factors. The stiffness was found not affected by number of load cycles after a distinct value. The results proposed here are in contrast with traditional solutions in the literature using the reduction factor in the soil resistance to tackle the complex situation.

References

Andersen, K.H., Murff, J.D., Randolph, M.F., Clukey, E., Erbrich, C., Jostad, H.P., Hansen, B., Aubeny, C., Sharma, P., Supachawarote, C., 2005. Suction anchors for deepwater applications. In: Proceedings of the INT Symposium on Frontiers in offshore Geotechniques (ISFOG). Keynote Lecture, Perth, Western Australian, pp. 3–30.

Andersen, L., Ibsen, L.B., Liingaard, M., 2008. Impedance of bucket foundations: torsional, horizontal and rocking motion. In: Papadrakakis, M., Topping, B.H.V. (Eds.), Proceedings of the Sixth International Conference on Engineering Computational Technology. Civil-Comp Press.

Banerjee, Pk, Butterfield, R., 1987. Dyn. Behav. Found. buried Struct., 270.

Barari, A., Ibsen, L.B., 2012. Undrained response of Bucket foundations to moment loading. Appl. Ocean Res. 36, 12–21.

Barari, A., Ibsen, L.B., 2014. Vertical capacity of Bucket foundations in undrained soil. J. Civil. Eng. Manag. 20 (3), 360–371.

Barari, A., Bayat, M., Saadati, M., Ibsen, L.B., Andersen, L.V., 2015. Transient analysis of Monopile foundations partially embedded in liquefied soil. Geomech. Eng. 8 (2), 257–282.

Bhattacharya, S., Lombardi, D., Muir Wood, D.M., 2011. Similitude relationships for physical modelling of monopile-supported offshore wind turbines. Int. J. Phys. Model. Geotech. 11 (2), 58–68.

Bhattacharya, S., Cox, J., Lombardi, D., Muir Wood, D., 2012. Dynamics of offshore wind turbines supported on two foundations. Proc. ICE—Geotech. Eng. 166 (2), 159–169.

Bienen, B., Byrne, B.W., Houlsby, G.T., Cassidy, M.J., 2006. Investigating six degree of freedom loading of shallow foundations on sand. Géotechnique 56 (6), 367–379.

Bransby, M.F., Randolph, M.F., 1999. The effect of embedment depth on the Undrained response of skirted foundations to combined loading. Soils Found. 39 (4), 19–33.

Butterfield, R., Houlsby, G.T., Gottardi, G., 1997. Standardised sign conventions and notation for generally loaded foundations. Geotechnique 47 (5), 1051–1054.

Cassidy, M.J., Byrne, B.W., Houlsby, G.T., 2002. Modelling the behaviour of circular footings under combined loading on loose carbonate sand. Géotechnique 52 (10), 705–712.

Cassidy, M.J., Byrne, B.W., Randolph, M.F., 2004. A comparison of the combined load behaviour of spudcan and caisson foundations on soft normally consolidated clay. Géotechnique 54 (2), 91–106.

Chen, R.P., Sun, Y.X., Zhu, B., Guo, W.D., 2015. Lateral cyclic pile–soil interaction studies on a rigid model monopile. Proc. Inst. Civil. Eng.-Geotech. Eng. 168 (GE2), 120–130.

Doherty, P., Gavin, K., 2011. Laterally loaded monopile design for offshore wind farms. Energy 165, 7–17.

Doherty, P., Gavin, K., 2012. Cyclic and rapid axial load tests on displacement piles in soft clay. J. Geotech. Geoenviron. Eng. 138 (8), 1022–1026.

Foglia, A., Ibsen, L.B., 2014. Monopod bucket foundations under cyclic lateral loading. Report-Aalborg University, (ISSN: 1901-7278).

Gazetas, G., 1975. In: Winterkorn, H.F., Fang, H.Y. (Eds.), Foundation Engineering Handbook. Van Nostrand Reinhold, New York.

Gazetas, G., 1983. Analysis of machine foundation vibrations: state-of-the-art. Soil Dyn. Earthq. Eng. 3 (1), 2–42.

Gourvenec, S., 2008. Effect of embedment on the undrained capacity of shallow foundations under general loading. Geotechnique 58 (3), 177–185.

Guo, W.D., Qin, H.Y., 2010. Thrust and bending moment of rigid piles subjected to moving soil. Can. Geotech. J. 47 (2), 180–196.

Houlsby, G.T., Cassidy, M.J., 2002. A plasticity model for the behaviour of footings on sand under combined loading. Géotechnique 52 (2), 117–129.

Ibsen, 2014. Frederikshavn (2002). Univer0073al Foundation Technical Workshop in Hamburg, Feb. 2014.

Ibsen, L.B., 2008. Implementation of a new foundations concept for Offshore Wind farms. In: Proceedings Nordisk Geoteknikermøte nr. 15 NGM 2008, 3–6 September 2008 Sandefjord, Norge, 1–15.

Ibsen, L.B., Larsen, K.A., Barari, A., 2014a. Calibration of failure criteria for Bucket foundations under general loading. J. Geotech. Geoenviron. Eng. ASCE. http://dx.doi.org/10.1061/(ASCE)GT.1943-5606.0000995.

Ibsen, L.B., Barari, A., Larsen, K.A., 2014b. An adaptive plasticity model for Bucket foundations. J. Eng. Mech. ASCE 140 (2), 361–373.

Ibsen, L.B., Barari, A., Larsen, K.A., 2015. Effect of embedment on the plastic behaviour of Bucket Foundations. J. Waterw. Port. Coast. Ocean Eng. ASCE. http://dx.doi.org/10.1061/(ASCE)WW.1943-5460.0000284.

Jardine, R.J., Standing, J.R., 2012. Field axial cyclic loading experiments on piles driven in sand. Soils Found. 52 (4), 723–736.

Kagawa, T., Kraft, L.M., 1980. Lateral load-deflection relationship of piles subjected to dynamic loadings. Soils Found. 20 (4), 19–36.

Larsen, K.A., Ibsen, L.B., Barari, A., 2013. Modified expression for the failure criterion of Bucket foundations subjected to combined loading. Can. Geotech. J. 50 (12), 1250–1259.

LeBlanc, C., Houlsby, G.T., Byrne, W., 2010. Response of stiff piles in sand to long-term cyclic lateral loading. Geotechnique 60 (2), 79–90.

Lombardi, D., 2010. Dynamics of Offshore Wind Turbines (M.Sc. Thesis). University of Bristol.

Luco, J.E., 1982a. Linear Soil-structure Interaction: A Review. Earthquake Ground Motion and its Effects on Structures. ASME, New York, N.Y., 41–57.

Lysmer, J., Richart, F.E., Jr., 1966. Dynamic response of footings to vertical loading. J. Soil Mech. Found. Div. 92 (1), 65–91.

Mita, A., Luco, J.E., 1989. Impedance functions and input motions for embedded square foundations. J. Geotech. Eng., ASCE 115 (4), 491–503.

Nielsen, O.J., 2014. The Universal Foundation. The Universal Foundation workshop. Hamburg, 25-26 February 2014.

Nova, R., Montrasio, L., 1991. Settlements of shallow foundations on sand. Geotechnique 41 (2), 243–256.

Rollins, K.M., Gerber, T.M., Kwon, K.H., 2009. Increased lateral abutment resistance from gravel backfills of limited width. J. Geotech. Geoenviron. Eng. 136 (1), 230–238.

Tjelta, T.I., 1995. Geotechnical experience from the installation of the Europipe jacket with bucket foundations. In: Proceedings Offshore Technology Conference, Houston, Texas, Paper No. 7795.

Villalobos, F.A., 2006. Model Testing of Foundations for Offshore Wind Turbines (D.Phil. Thesis). Univ. of Oxford, Oxford, U.K.

Zhu, B., Byrne, B.W., Houlsby, G.T., 2013. Long-term lateral cyclic response of suction caisson foundations in sand. J. Geotech. Geoenviron. Eng. 139, 73–83.